Additive and nonadditive models of vapor-liquid equilibrium in CO_2 from first principles

Mark T. Oakley and Richard J. Wheatley[a)]
School of Chemistry, University of Nottingham, University Park, Nottingham NG7 2RD, United Kingdom

(Received 15 August 2008; accepted 9 December 2008; published online 21 January 2009)

We describe quantum-chemical calculations on dimers of CO_2 and use the results to develop first-principles models for Gibbs ensemble Monte Carlo simulations of the phase coexistence curve. Isotropic pairwise potentials are insufficient to model the phase behavior and overestimate the binding in liquid CO_2 by 4 kJ mol^{-1}. An anisotropic treatment of the atoms in the pairwise potential reduces the strength of the binding by ~0.5 kJ mol^{-1}. We use *ab initio* calculations on trimers of CO_2 to assess the strength of nonadditive interactions. Including nonadditive dispersion in Gibbs ensemble simulations gives an enthalpy of vaporization within 1.5 kJ mol^{-1} of the experimental value over a wide range of temperatures. © *2009 American Institute of Physics*.
[DOI: 10.1063/1.3059008]

I. INTRODUCTION

Supercritical CO_2 has been used in a variety of industrial processes, from decaffeinating coffee to extracting oil from wells. It is also useful as a green alternative to organic solvents in many chemical processes.[1] Supercritical CO_2 is a particularly good solvent for fluorinated compounds,[2] and such mixtures have been used as refrigerants. The phase behavior of CO_2 has been the subject of many experimental studies and the properties of pure CO_2 (Ref. 3) and mixtures with other compounds[2,4] are well established. The solvent properties of supercritical CO_2 are not completely understood, and molecular simulations offer insight into the fundamental forces involved. The development of a good model of pure CO_2 is an important step in understanding its behavior as a solvent.

A widely used intermolecular potential for CO_2 is the elementary physics model (EPM).[5,6] This potential includes pairwise interactions between all atoms with a Coulomb and a Lennard-Jones component,

$$U = \sum_{a,b} \left[\frac{q_a q_b}{r_{ab}} + \frac{A_{ab}}{r_{ab}^{12}} - \frac{B_{ab}}{r_{ab}^{6}} \right], \tag{1}$$

where r_{ab} is the separation between atoms a and b. The atomic charges (q_a, q_b) reproduce the experimental quadrupole moment and the van der Waals parameters (A_{ab}, B_{ab}) are fitted to reproduce the experimental pressure and internal energy at 239 K.

The EPM potential reproduces the phase properties of CO_2 well, but it is fitted to the phase properties of pure CO_2 at one temperature and may not be applicable under different conditions. This could be especially important when modeling mixtures of CO_2 with other compounds, where the arrangement of CO_2 molecules around solutes could be significantly different to their arrangement in the pure fluid. It is desirable to model CO_2 using parameters based entirely on first-principles calculations, because such models can be used beyond the conditions where empirical potentials are fitted. Additionally, the methods used to develop models of CO_2 can be applied to other systems where no experimental data are available.

Two recent potentials, BBV and SAPT-s, were fitted to *ab initio* calculations on the CO_2 dimer using second-order Møller–Plesset perturbation theory (MP2) (Ref. 7) and symmetry adapted perturbation theory,[8] respectively. Both of these potentials include atomic charges. The SAPT-s potential also uses r^{-6} and r^{-8} terms for the van der Waals interactions, whereas the BBV potential has r^{-6}, r^{-8}, r^{-10}, and r^{-12} terms. Both potentials include dummy atoms on the CO bond to improve the fitting of the dimer potential energy surface. Both of these potentials have been used in Gibbs ensemble molecular dynamics simulations.[9] In these simulations, the BBV potential more closely reproduces the experimental densities and critical temperature.

All of the potentials discussed so far ignore the explicit effect of multibody interactions, which have a significant effect on the structure and energetics of many systems.[10] In noble gases, nonadditive dispersion accounts for 5%–10% of the total energy of the liquid phase.[11–13] Nonadditive exchange repulsion may also be important in these systems. In water, the nonadditive dispersion energy is very small, but nonadditive induction accounts for about 15% of the total energy in liquid phase and has a significant effect on its structure.[14,15]

In this paper, we present pairwise potentials fitted to high-level quantum-chemical calculations on the CO_2 dimer and explore the effect of the choice of quantum-chemical method and the form of the fitted potential. We also present calculations on the CO_2 trimer and show that nonadditivity accounts for an important part of the total interaction energy.

[a)]Electronic mail: richard.wheatley@nottingham.ac.uk.

 © 2009 American Institute of Physics

Downloaded 02 Jul 2009 to 128.243.220.22. Redistribution subject to AIP license or copyright; see http://jcp.aip.org/jcp/copyright.jsp

TABLE I. Parameters in the isotropic MP2 potentials. All quantities are in a.u.

Basis set	aug-cc-pVDZ	aug-cc-pVTZ	aug-cc-pVQZ	Complete basis
rms fit error (μE_h)	145	138	138	136
q_C	0.575	0.541	0.534	0.568
q_O	−0.288	−0.271	−0.267	−0.284
A_{CC}	3.08×10^5	2.57×10^5	2.60×10^5	2.31×10^5
A_{CO}	6.89×10^5	6.05×10^5	5.88×10^5	6.01×10^5
A_{OO}	1.12×10^6	1.10×10^6	1.08×10^6	1.05×10^6
B_{CC}	−69.8	−70.0	−72.3	−78.2
B_{CO}	42.8	46.0	47.9	50.9
B_{OO}	24.3	25.8	25.7	24.7

II. METHODS

A. Additive potentials

In all calculations, the CO_2 molecule is considered to be rigid. This gives the CO_2 dimer potential energy surface four degrees of freedom: R, the C–C separation, ϑ_A and ϑ_B, the angles between the molecular z axes and the vector joining the two carbon atoms, and ϕ, the O–C–C–O dihedral angle. Geometries for *ab initio* calculations are generated with values of R in $0.5a_0$ steps between $5.0a_0$ and $13.0a_0$. The ϑ_A and ϑ_B angles are varied in steps of $\pi/16$ rad and ϕ is varied in steps of $\pi/8$ rad. Any geometry where two atoms in different molecules are separated by less than $5.0a_0$ is rejected. This scheme leads to 2414 points for *ab initio* calculation of the potential energy surface.

The interaction energy of the CO_2 dimer is evaluated at each of these 2414 points using the MP2 method as implemented in MOLPRO.[16] In these calculations, counterpoise correction is used to remove the basis-set superposition error. These calculations are performed using Dunning's aug-cc-pVDZ, aug-cc-pVTZ, and aug-cc-pVQZ basis sets.[17] An extrapolation to the complete basis-set limit is performed at each point by an exponential fit to the double-, triple- and quadruple-zeta energies. Core correlation effects could influence the interaction energies. Therefore the dimer energies are also evaluated with the aug-cc-pCVTZ polarized core basis set.[18]

Coupled cluster methods treat correlation better than MP2, but they are much more computationally demanding and calculations on all 2414 geometries with an adequate basis set are impractical. Therefore, a smaller set of 50 structures is chosen from a Monte Carlo simulation of liquid CO_2 at 268 K. A pair of molecules is chosen at random from a random time step in the simulation, with a probability proportional to R^{-2} to give preference to closely separated molecules. The interaction energies of these 50 dimers are evaluated at the CCSD(T)/aug-cc-pVTZ level and at the MP2/aug-cc-pVTZ level for comparison.

The geometry of CO_2 may have an effect on the calculated energies. Calculations at the MP2/aug-cc-pVTZ level are performed on the same 50 CO_2 dimers with different C–O bond lengths. The chosen lengths are the EPM2 bond length (1.149 Å), the experimental equilibrium bond length r_0 (r_0=1.1615 Å), and the experimental vibrationally averaged bond length (r_e=1.1632 Å).[19]

A charge plus Lennard-Jones potential [Eq. (1)] is fitted to each set of *ab initio* calculations (Table I). The parameter fits are performed by least-squares minimization using a Boltzmann-weighting scheme with a temperature of 298 K. The typical rms error in the fits to the 2414 points is 140 μE_h. Therefore there is scope for increasing the accuracy of the fit by the introduction of more parameters.

The atoms of the CO_2 molecule are anisotropic and a purely spherical treatment of the atoms is insufficient to model the potential energy surface. The BBV (Ref. 7) and

TABLE II. Parameters in the anisotropic MP2 potentials. All quantities are in a.u.

Basis set	aug-cc-pVDZ	aug-cc-pVTZ	aug-cc-pVQZ	Complete basis
rms fit error (μE_h)	94	75	59	71
q_C	0.654	0.576	0.562	0.555
q_O	−0.327	−0.288	−0.281	−0.277
A_{CC}	4.45×10^5	2.98×10^5	2.80×10^5	2.38×10^5
A_{CO}	4.71×10^5	4.52×10^5	4.55×10^5	4.76×10^5
A_{OO}	1.39×10^6	1.32×10^6	1.28×10^6	1.24×10^6
B_{CC}	−151	−153	−156	−163
B_{CO}	91.3	95.3	97.8	101.0
B_{OO}	3.80	2.96	3.35	4.55
$A_{CO(011;00)}$	-1.02×10^6	-9.90×10^5	-9.83×10^5	-9.72×10^5
$A_{OO(011;00)}$	9.66×10^5	9.18×10^5	8.98×10^5	8.87×10^5
$A_{OO(101;00)}$	9.66×10^5	9.18×10^5	8.98×10^5	8.87×10^5
$A_{OO(110;00)}$	-6.44×10^4	-5.37×10^4	-5.28×10^4	-5.89×10^4
$A_{OO(112;00)}$	-2.96×10^5	-2.43×10^5	-2.40×10^5	-2.28×10^5

Downloaded 02 Jul 2009 to 128.243.220.22. Redistribution subject to AIP license or copyright; see http://jcp.aip.org/jcp/copyright.jsp

SAPT (Ref. 8) potentials deal with this anisotropy by introducing dummy atoms between the C and O atoms. Here, an alternative approach is taken and anisotropic atom-atom r^{-12} terms are added to the pairwise potential using spherical tensors.[20] The anisotropic potential for a pair of molecules, A and B, takes the form

$$U_{AB} = \sum_{a\in A}\sum_{b\in B}\left[\frac{q_a q_b}{r_{ab}} + \frac{A_{ab}}{r_{ab}^{12}} - \frac{B_{ab}}{r_{ab}^{6}} + \frac{A_{ab(011;00)}\mathbf{b}\cdot\hat{\mathbf{R}}}{r_{ab}^{12}\sqrt{3}} + \frac{A_{ab(101;00)}\mathbf{a}\cdot\hat{\mathbf{R}}}{r_{ab}^{12}\sqrt{3}} + \frac{A_{ab(110;00)}\mathbf{a}\cdot\mathbf{b}}{r_{ab}^{12}\sqrt{3}} + \frac{A_{ab(112;00)}(\mathbf{a}\cdot\mathbf{b} - 3\times\mathbf{a}\cdot\hat{\mathbf{R}}\times\mathbf{b}\cdot\hat{\mathbf{R}})}{r_{ab}^{12}\sqrt{30}}\right], \quad (2)$$

where $\mathbf{a}$ and $\mathbf{b}$ are unit vectors along the atomic z axes of atoms a and b (which are aligned with the C–O bonds) and $\hat{\mathbf{R}}$ is a unit vector giving the direction from atom a to b. All seven terms from this potential are used to evaluate the energies of O–O interactions but only the first four for C–O interactions and the first three for C–C interactions. The inclusion of anisotropic terms reduces the rms fitting error to about 70 μE_h (Table II). Anisotropic potentials are not generated for the sets of calculations where only 50 geometries are available because of overfitting of the potential energy surface.

The potential energy surface calculated by extrapolation to the complete basis-set limit is considered to be the best available. The isotropic and anisotropic fits to this surface are referred to as CBS-i and CBS-a, respectively.

B. Nonadditive *ab initio* calculations

The nonadditive energy of a trimer, U_3, is defined as the difference between the interaction energy of a trimer and the sum of its component dimer interaction energies,

$$U_{ABC} = U_{AB} + U_{AC} + U_{BC} + U_3. \quad (3)$$

The CO_2 trimer has nine degrees of freedom, which is too many to allow *ab initio* calculations that cover the whole potential energy surface. Instead, 250 trimer geometries are chosen from the most highly populated areas of the conformational space by selecting trimers from a simulation of liquid CO_2 at 268 K. They are generated by selecting a molecule at random from a random step in the simulation, then choosing two more molecules at random with an atom within 4 Å of an atom in the first molecule. The nonadditive interaction energies of these 250 trimers are evaluated at the MP2/aug-cc-pVTZ level. Counterpoise correction is used to remove the basis-set superposition error in these calculations.

The MP2 method does not include the effects of nonadditive dispersion and calculations using other methods must be performed to obtain this. Here, the nonadditive dispersion energy is calculated with the SAPT method,[21] but with the SAPT wave function, $\Psi^{(1;0)}_{\mathrm{disp},AB}$ (the first-order uncoupled Hartree–Fock wave function), replaced by the corresponding first-order coupled Hartree–Fock wave function. There is no basis-set superposition error in these calculations and they are much less computationally demanding than the MP2 trimer calculations. Therefore, they are performed with a larger (aug-cc-pVQZ) basis set.

Coupled cluster calculations also include the effect of nonadditive dispersion but are prohibitively expensive when using a large basis set. The best coupled cluster calculations we can perform are CCSD(T)/aug-cc-pVDZ. The nonadditive energies of the first 10 trimers from the set of 250 are evaluated with this method, with MP2 and SAPT calculations performed with the same basis set for comparison.

These ten structures divide into two groups. In the first, the difference between the CCSD(T) and MP2 energies is less than 10 μE_h. In the second group, the centers of the molecules form an acute triangle and the CCSD(T) energies are more repulsive than the MP2 energies by up to 50 μE_h. Adding the nonadditive dispersion energy to the nonadditive MP2 energy reproduces the nonadditive CCSD(T) energy, with a difference of less than 10 μE_h in all cases. Thus, the combination of nonadditive MP2 and nonadditive SAPT dispersion is a good model of the total nonadditive energy.

C. Nonadditive potentials

Fits to the trimer potential are needed if the effects of nonadditivity on the phase properties of CO_2 are to be evaluated using simulations. The nonadditive energy is considered as the sum of dispersion, induction, and "exchange-repulsion" components,

$$U_3 = U_{3,\mathrm{disp}} + U_{3,\mathrm{ind}} + U_{3,\mathrm{exch}}. \quad (4)$$

The SAPT nonadditive dispersion energy is fitted to the Axilrod–Teller triple dipole dispersion energy,[22]

$$U_{3,\mathrm{disp}} = \frac{1}{6}\sum_{a,b,c}\nu_{abc}(1 + 3\cos\theta_a\cos\theta_b\cos\theta_c)r_{ab}^{-3}r_{ac}^{-3}r_{bc}^{-3}, \quad (5)$$

where atoms a, b, and c are in different molecules and ν_{abc} is the nonadditivity coefficient for those atoms. These parameters are fitted as a geometric progression between ν_{CCC} and ν_{OOO} ($\nu^3_{\mathrm{CCO}} = \nu^2_{\mathrm{CCC}}\nu_{\mathrm{OOO}}$ and $\nu^3_{\mathrm{COO}} = \nu_{\mathrm{CCC}}\nu^2_{\mathrm{OOO}}$).

The nonadditive induction energy is not fitted but is represented as

$$U_{3,\mathrm{ind}} = \frac{1}{2}\sum_{a,b,c} -\mathbf{F}_{ab}\cdot\boldsymbol{\alpha}_b\cdot\mathbf{F}_{cb}, \quad (6)$$

where α_b is the atomic polarizability of atom b and $\mathbf{F}_{ab}$ is the electric field produced at atom b by atom a. If the polarizability is treated isotropically, this simplifies to

$$U_{3,\mathrm{ind}} = \frac{1}{2}\sum_{a,b,c} -q_a q_c\alpha_b r_{ab}^{-2}r_{bc}^{-2}\cos\theta_b, \quad (7)$$

where q is the atomic charge, r is the distance between two atoms, and θ_b is the angle made by atoms a, b, and c. No parameter fitting is required because the atomic charges and polarizabilities are obtained from *ab initio* calculations on a single CO_2 molecule. The atomic charges are fitted to reproduce the MP2/aug-cc-pVTZ quadrupole moment ($q_C = 0.593$,

Downloaded 02 Jul 2009 to 128.243.220.22. Redistribution subject to AIP license or copyright; see http://jcp.aip.org/jcp/copyright.jsp

TABLE III. The effect of system size on the heat of vaporization of CO_2. Values in parentheses are the uncertainties at the 95% confidence level.

Number of molecules	333	667
ΔH_{vap}^{228} (kJ mol^{-1})	17.31(0.07)	17.33(0.02)
ΔH_{vap}^{258} (kJ mol^{-1})	15.15(0.05)	15.21(0.03)
ΔH_{vap}^{288} (kJ mol^{-1})	12.57(0.04)	12.53(0.03)

q_O=−0.297). The atomic polarizabilities are calculated at the MP2/aug-cc-pVTZ level using a recently developed method.[23] The polarizabilities are 13.045 a.u. along the CO bond and 5.021 a.u. along the other two axes for carbon. For oxygen, the polarizabilities are 13.501 a.u. along the CO bond and 5.308 a.u. along the other two axes. The isotropic polarizablities are 7.706 a.u. for carbon and 8.039 a.u. for oxygen.

The nonadditive induction energies are all evaluated without iterating the induced moments. A self-consistent treatment of nonadditive induction may be more satisfactory. However, the nonadditive induction here is small, with energy less than 150 μE_h. This would give rise to small changes in the atomic charges and have little influence on the total energy.

The nonadditive exchange repulsion is calculated by subtracting nonadditive dispersion and induction energies given by Eqs. (5) and (6) from the sum of the nonadditive MP2 and SAPT dispersion energies. This is fitted to

$$U_{3,\mathrm{exch}} = \frac{1}{6}\sum_{a,b,c} [A_{abc}\exp(-B_{abc}r_{ab} - B_{bca}r_{bc} - B_{cab}r_{ac}) + C_{abc}\exp(-D_{abc}r_{ab} - D_{cba}r_{bc})\cos\theta_b]. \quad (8)$$

A potential with a similar form has previously been used to fit the nonadditive exchange-repulsion energies of He_3 and H_3.[24] Different values of A and C are fitted for each combination of atoms, but only one value is used for each of B and D to reduce the complexity of the nonlinear part of the fit. The parameters A and C are fitted by least-squares minimization with fixed values of B and D. Several fits are performed with different values of B and D, but the quality of the fit is insensitive to these two parameters and both are fixed at 2 a.u. in the results presented here.

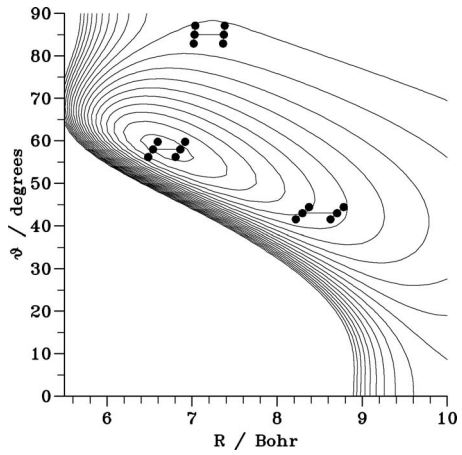

FIG. 1. The CO_2 dimer potential energy surface from the isotropic fit to the MP2/aug-cc-pVQZ energies. The molecules are parallel, with $\vartheta_a = \vartheta_b$ and ϕ=0.

TABLE IV. Properties of the CO_2 dimer at its minimum energy.

Pair potential	r_{CC} (Å)	υ (deg)	U (μE_h)
aug-cc-pVDZ (isotropic)	3.75	54	−1625
aug-cc-pVTZ (isotropic)	3.64	56	−1862
aug-cc-pVQZ (isotropic)	3.60	56	−1964
CBS-i	3.59	64	−2029
aug-cc-pVDZ (anisotropic)	3.67	57	−1698
aug-cc-pVTZ (anisotropic)	3.56	54	−1969
aug-cc-pVQZ (anisotropic)	3.53	58	−2083
CBS-a	3.51	58	−2151
EPM[a]	3.71	56	−1856
BBV[b]	3.47	60	−2200
SAPT-s[c]	3.57	58	−2142

[a]Reference 5.
[b]Reference 7.
[c]Reference 8.

D. Gibbs ensemble simulations

Gibbs ensemble Monte Carlo is a widely used method of studying the phase behavior of fluids.[25] In this ensemble, simulations on the liquid and gas phases are performed simultaneously. The Monte Carlo move list includes translations and rotations of molecules. In addition, the chemical potentials of the two boxes are equalized by transferring molecules between boxes and the pressure is equalized by changing the volumes of the boxes. In the *NVT* Gibbs ensemble the total volume of the system cannot change and an increase in the volume of one phase must be matched by a decrease in the volume of the other.

Gibbs ensemble Monte Carlo simulations are performed using all of the previously described additive potentials. Simulations are performed at temperatures at 10 K intervals between 228 and 288 K. The total volume of the system is chosen to give roughly equal partitioning of the molecules between the liquid and gas phases. All simulations consist of 200 000 Monte Carlo passes, with each pass comprising an average of one translation or rotation per molecule plus 100 swap moves and 1 volume move. The first 20 000 passes in each simulation are used for equilibration of the system. The

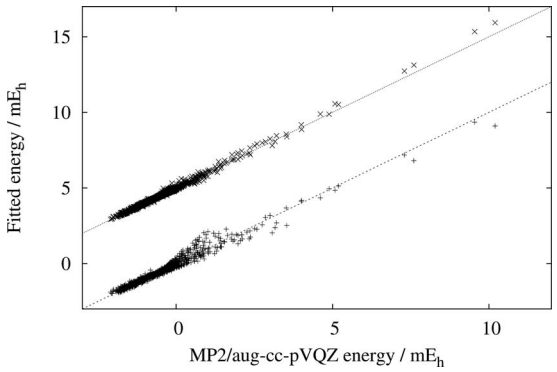

FIG. 2. The CBS-i (+) and CBS-a (×) fits to the CO_2 dimer potential energy surface. The CBS-a fit is shifted by 5 mE_h for clarity.

Downloaded 02 Jul 2009 to 128.243.220.22. Redistribution subject to AIP license or copyright; see http://jcp.aip.org/jcp/copyright.jsp

TABLE V. The phase properties of CO_2 calculated with isotropic MP2 and CCSD(T) potentials. Values in parentheses are the uncertainties at the 95% confidence level.

	Experiment	MP2/aug-cc-pVDZ	MP2/aug-cc-pVTZ	MP2/aug-cc-pVQZ	CBS-i	CCSD(T)/aug-cc-pVTZ
ΔH_{vap}^{228} (kJ mol^{-1})	14.49	10.54(0.04)	15.63(0.03)	17.33(0.02)	18.28(0.03)	16.20(0.06)
ΔH_{vap}^{258} (kJ mol^{-1})	12.07	6.04(0.24)	13.28(0.04)	15.21(0.03)	16.24(0.04)	13.47(0.05)
ΔH_{vap}^{288} (kJ mol^{-1})	7.81	⋯	10.01(0.06)	12.53(0.03)	13.71(0.06)	9.56(0.09)
ρ_l^{228} (kg m^{-3})	1134.9	973.8(2.3)	1182(2)	1247(1)	1280(1)	1203(2)
ρ_l^{258} (kg m^{-3})	1006.1	737.5(21.3)	1067(2)	1143(1)	1180(2)	1071(3)
ρ_l^{288} (kg m^{-3})	824.4	⋯	918.8(3.4)	1016(3)	1062(2)	888.2(8)
ρ_g^{228} (kg m^{-3})	21.8	65.8(2.3)	17.8(0.9)	11.9(0.5)	8.7(0.8)	19.3(1.6)
ρ_g^{258} (kg m^{-3})	60.2	188.1(20.5)	49.3(1.6)	32.7(0.8)	25.8(1.0)	53.9(2.2)
ρ_g^{288} (kg m^{-3})	160.7	⋯	119.3(3.5)	76.7(2.2)	60.9(2.2)	132.1(4.1)
P_{228} (bar)	8.2	22.1(0.6)	7.0(0.3)	4.8(0.2)	3.6(0.3)	7.6(0.5)
P_{258} (bar)	22.6	52.4(1.8)	19.8(0.6)	13.9(0.3)	11.2(0.3)	21.5(0.7)
P_{288} (bar)	50.2	⋯	44.4(1.1)	32.2(0.7)	26.6(0.7)	48.4(0.9)

uncertainties in the simulated properties are calculated from the standard deviations of block averages. The production stage of each simulation is split into ten blocks for the calculation of uncertainties.

To test the stability of the Gibbs ensemble simulations, test calculations are performed using the isotropic quadruple-zeta potential in simulations of 333 and 667 molecules (Table III). There is good agreement between phase properties with both system sizes, and all further calculations are performed with 667 molecules.

In all simulations a cutoff r_{cut} of 12 Å between the carbon atoms is used; the pair potential is set to zero for larger R. The r^{-6} term still makes a significant contribution to the energy at this distance, so a long-range correction is used where the long-range energy of a molecule is given by

$$U_{\text{long-range}} = \tfrac{4}{3}\pi\rho B r_{\text{cut}}^{-3}. \tag{9}$$

There is no need to correct for long-range Coulombic interactions because the CO_2 molecule has no dipole. The r^{-12} term decays at short distance, so a correction to this term is also unnecessary.

During all Gibbs ensemble simulations, the pair of molecules with the lowest energy is recorded. Given the large number of pair energy evaluations in a simulation, this should be close to the most stable arrangement on the dimer potential energy surface.

The evaluation of the nonadditive energies is too computationally demanding to perform at every step in the Monte Carlo simulation. To estimate the nonadditive contribution, the nonadditive energies of the liquid and gas phases are calculated after every 1000 passes using Eqs. (5), (6), and (8). These calculations show that the nonadditive dispersion energy correlates well with $\rho^{2.5}$. A further set of Gibbs ensemble simulations is therefore performed using an effective nonadditive potential where the total energy of a phase is given by

$$U_{\text{nonadd}} = \sum_{i<j} U_{\text{pair},ij} + nk\rho^{2.5}. \tag{10}$$

The pairwise energy is calculated using the CBS-i and CBS-a potentials. The explicit calculation of nonadditive energies is replaced by the second term, where n is the number of molecules in the phase and k is a constant fitted to reproduce the nonadditive dispersion energies.

III. RESULTS AND DISCUSSION

A. Additive potentials

The CO_2 dimer potential energy surface from our calculations (Fig. 1) is comparable to previous *ab initio* calculations,[7,8] with the most stable structure being a slipped parallel geometry. As the size of the basis set increases, the strength of the binding between CO_2 molecules increases and the C–C contact shifts to a shorter distance (Table IV). Both of these observations are consistent with previous studies on the effect of the basis set.[7] The isotropic potentials fit the dimer energies poorly on the low repulsive wall (Fig. 2). The inclusion of anisotropic terms in the potential corrects the poor agreement between the energies for close O–O contacts and substantially reduces the fitting error. The most stable structures from the anisotropic potentials are more strongly bound and in closer contact than in the isotropic potential. The most stable structure from the CBS-a potential is similar in geometry and energy to the most stable structures from the BBV and SAPT-s potentials.

The basis set also has a significant effect when the fitted potentials are used in Gibbs ensemble simulations. As the size of the basis set increases, the stronger binding leads to higher liquid densities and higher enthalpies of vaporization. The corresponding vapor pressures and gas phase densities decrease as the basis-set size increases (Table V). The double-zeta basis substantially underestimates the CO_2 interaction energy, with the simulations above 248 K converging poorly due to its proximity to the critical point. The triple-zeta potential is close to reproducing the experimental properties, but the larger basis sets bind the CO_2 together even more strongly. From these results, the isotropic MP2 dimer potentials overestimate the strength of the CO_2 interaction.

The anisotropic potentials all give lower enthalpies of vaporization than their isotropic counterparts by ~0.5 kJ mol^{-1} (Table VI). The inclusion of anisotropic terms increases the central processing unit time required for

Downloaded 02 Jul 2009 to 128.243.220.22. Redistribution subject to AIP license or copyright; see http://jcp.aip.org/jcp/copyright.jsp

TABLE VI. The phase properties of CO_2 calculated with anisotropic MP2 potentials. Values in parentheses are the uncertainties at the 95% confidence level.

	Experiment	aug-cc-pVDZ	aug-cc-pVTZ	aug-cc-pVQZ	CBS-a
ΔH_{vap}^{228} (kJ mol^{-1})	14.49	10.23(0.06)	15.31(0.02)	16.94(0.04)	17.85(0.03)
ΔH_{vap}^{258} (kJ mol^{-1})	12.07	···	12.85(0.03)	14.73(0.02)	15.79(0.06)
ΔH_{vap}^{288} (kJ mol^{-1})	7.81	···	9.36(0.06)	11.90(0.06)	13.13(0.04)
ρ_l^{228} (kg m^{-3})	1134.9	958.2(2.5)	1172(1)	1235(2)	1267(1)
ρ_l^{258} (kg m^{-3})	1006.1	···	1050(1)	1128(2)	1168(2)
ρ_l^{288} (kg m^{-3})	824.4	···	889.4(5.0)	998.4(3.7)	1046(3)
ρ_g^{228} (kg m^{-3})	21.8	69.2(2.2)	19.3(0.8)	13.1(0.5)	10.0(0.7)
ρ_g^{258} (kg m^{-3})	60.2	···	51.8(1.4)	36.1(1.0)	28.8(1.4)
ρ_g^{288} (kg m^{-3})	160.7	···	127.8(3.9)	85.2(2.9)	68.1(1.9)
P_{228} (bar)	8.2	22.4(0.6)	7.5(0.3)	5.2(0.2)	4.1((0.3)
P_{258} (bar)	22.6	···	20.3(0.3)	14.9(0.3)	12.3(0.5)
P_{288} (bar)	50.2	···	44.7(0.8)	33.6(0.6)	28.4(0.6)

the Gibbs ensemble simulation by a factor of ~2, which represents a worthwhile gain in accuracy for only a moderate increase in computational cost.

The dimer energies calculated with the aug-cc-pVTZ and aug-cc-pCVTZ basis sets are almost identical, with rms difference of 5 μE_h. Therefore, core-valence correlation does not make a significant contribution to the dimer potential energy surface. Changing the C–O bond length has a slightly larger but still insignificant effect, with a rms difference of 17 μE_h between potential energy surfaces with C–O bond lengths of 1.149 and 1.1632 Å. Fitted potentials with different C–O bond lengths all give similar phase properties when they are used in Gibbs ensemble simulations (Table VII).

The potential fitted to CCSD(T)/aug-cc-pVTZ is more repulsive than the MP2/aug-cc-pVTZ potential at low temperatures. As the temperature increases, this difference decreases until at 288 K the phase properties from both potentials are almost identical.

B. Nonadditivity in the CO_2 trimer

The total interaction energies of the CO_2 trimers are typically between −3 and −1 mE_h. The nonadditive energies, calculated as the sum of the nonadditive MP2 and nonadditive dispersion energies, range from −0.1 to 0.2 mE_h. The extreme examples in this range occur when there is at least one triangle of atoms where all three sides are short (less than 3 Å), and in most geometries the nonadditive energies are an order of magnitude smaller.

The nonadditive dispersion energies of the trimers are mainly between −5 and 60 μE_h, with a mean value of 9 μE_h. This preference for positive values is to be expected.

TABLE VII. The effect of the C–O bond length on the phase properties of CO_2. Potentials are fitted to MP2/aug-cc-pVTZ calculations on 50 CO_2 dimers. Values in parentheses are the uncertainties at the 95% confidence level.

r_{CO} (Å)	1.149	1.1615	1.1632
ΔH_{vap}^{258} (kJ mol^{-1})	13.01(0.05)	13.00(0.06)	13.03(0.04)
ρ_l^{258} (kg m^{-3})	1068(3)	1062(2)	1066(2)
ρ_g^{258} (kg m^{-3})	55.0(2.1)	53.0(1.5)	54.6(1.8)
P_{258} (bar)	20.7(0.6)	21.2(0.4)	21.7(0.6)

When three atoms are in close contact and form an equilateral triangle, the $(1+3\cos\theta_a\cos\theta_b\cos\theta_c)$ term in Eq. (5) is positive, leading to a positive energy. When three atoms are collinear, $(1+3\cos\theta_a\cos\theta_b\cos\theta_c)$ takes its largest negative value, but one of the values of r must be larger, leading to a smaller negative energy.

The best fit to the dispersion energy is obtained with $\nu_{CCC}=0.4$ a.u. and $\nu_{OOO}=209$ a.u., with a rms error of 3.6 μE_h (Table VIII). If ν_{CCC} and ν_{OOO} are varied between 0 and 3000 a.u., the quality of the dispersion fit depends strongly on $\nu_{CO_2CO_2CO_2}$,

$$\nu_{CO_2CO_2CO_2} = \nu_{CCC} + 6\nu_{CCO} + 12\nu_{COO} + 8\nu_{OOO}, \tag{11}$$

but it is less sensitive to the values of the individual atomic nonadditivity coefficients. For example, an alternative fit with $\nu_{CCC}=\nu_{OOO}=76.2$ only has a slightly worse rms fitting error of 4.2 μE_h. The value $\nu_{CO_2CO_2CO_2}$ from the best parameter fit (1993 a.u.) is in good agreement with the value of 1970 a.u. obtained from the CO_2 dipole oscillator strength distribution.[26]

The Axilrod–Teller equation only includes the effect of dipole-dipole-dipole dispersion and terms involving higher multipoles could contribute to the energy. However, calculations on noble gases show that higher-order interactions are smaller in magnitude than the triple dipole term and alternate in sign, with the Axilrod–Teller energy close to the total three body dispersion.[8] The Axilrod–Teller equation reproduces the nonadditive dispersion energy of CO_2 very well, with a rms error of about 4 μE_h. Therefore, the effort of including elaborate higher multipole terms is probably not justified.

The nonadditive MP2 energies range from −130 to 100 μE_h. Unlike the dispersion, there is no preference for positive or negative values, so these cancel and give a mean

TABLE VIII. Fitted Axilrod–Teller nonadditivity coefficients of CO_2 in a.u.

ν_{CCC}	0.4	76.2
ν_{CCO}	3.0	76.2
ν_{COO}	25.2	76.2
ν_{OOO}	209.0	76.2
$\nu_{CO_2CO_2CO_2}$	1993	2056
rms error (μE_h)	3.6	4.2

Downloaded 02 Jul 2009 to 128.243.220.22. Redistribution subject to AIP license or copyright; see http://jcp.aip.org/jcp/copyright.jsp

TABLE IX. Parameters obtained by fitting the nonadditive exchange-repulsion energy.

A_{CCC}	-3.12×10^{14}
A_{CCO}	2.15×10^{12}
A_{COO}	7.81×10^{10}
A_{OOO}	-2.53×10^{10}
B	2.0
C_{CCC}	3.83×10^{7}
$C_{CCO,OCC}$	-6.32×10^{6}
C_{COC}	2.74×10^{6}
$C_{COO,OOC}$	-6.79×10^{5}
C_{OCO}	9.54×10^{4}
C_{OOO}	-8.78×10^{4}
D	2.0

nonadditive MP2 energy of 2 μE_h. The nonadditive induction energies calculated using Eq. (6) or Eq. (7) are in good agreement with the nonadditive MP2 energies, with rms differences of 12.6 and 13.5 μE_h, respectively. Much of the difference between the MP2 energies and the energies from Eq. (6) is due to trimers with short interatomic contacts where exchange repulsion becomes important.

The nonadditive exchange-repulsion energy is calculated by subtracting the nonadditive dispersion energy from the best parameter fit to Eq. (5) and nonadditive induction energy calculated using Eq. (6) from the total nonadditive energy of a trimer. The exchange-repulsion energy therefore includes mixed terms such as exchange induction and exchange dispersion, higher-order perturbative terms, and fitting errors from the other terms. The rms error in the exchange-repulsion fit is 10 μE_h (Table IX).

The total nonadditive energy from Eqs. (5), (6), and (8) is a good fit to the total *ab initio* nonadditive energies, with a rms error of 10 μE_h (Fig. 3).

C. Nonadditivity in the phase behavior of CO_2

The nonadditive energies are calculated every 1000 passes during simulations using the CBS-a potential. When the nonadditive energy of a trimer is evaluated, the longest of the three distances between the molecular centers is considered. If this distance is less than a certain cutoff distance, the trimer's nonadditive energy is added to the total energy of the system. Cutoff distances up to half of the length of the liquid box are considered. The length of the liquid box varies during the simulations, but it never drops below 28 Å. Therefore, the largest cutoff considered is 14 Å. At this distance, the nonadditive induction and exchange-repulsion energies have converged and the nonadditive dispersion is close to convergence (Fig. 4). The nonadditive energy with a cutoff of 14 Å is therefore taken as the total nonadditive energy (Table X).

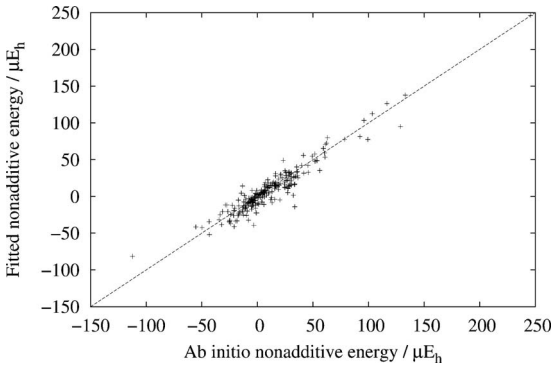

FIG. 3. The nonadditive energy of 250 CO_2 trimers from *ab initio* calculations and from Eqs. (5), (6), and (8).

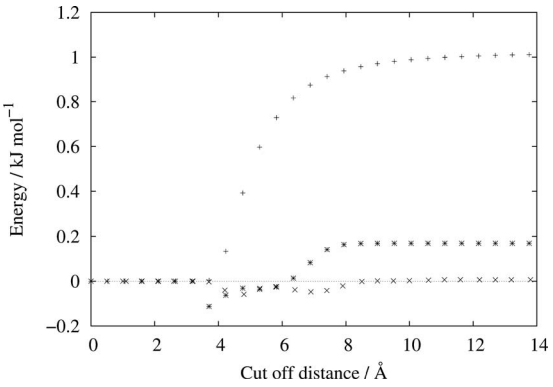

FIG. 4. The nonadditive dispersion (+), induction (×), and exchange-repulsion (∗) energies in the liquid phase from a simulation at 228 K using the CBS-a potential.

Nonadditive dispersion makes a repulsive contribution to the total energy and adds more than 1 kJ mol^{-1} at 228 K. The nonadditive induction energy is much smaller than the dispersion. The induction energy in a given trimer is of similar magnitude to the dispersion, but positive and negative induction energies cancel when a large number of trimers are considered. The isotropic treatment of induction gives total energies that are about three times larger than the anisotropic energies, but these are still small when compared to the nonadditive dispersion energies. Nonadditive exchange repulsion also makes a small repulsive contribution to the energy. The nonadditive dispersion and induction energies vary little through the course of a simulation and the standard errors in both properties are small. There is more variation in the nonadditive exchange repulsion, but the standard errors are still small when compared to the total nonadditive energy.

The nonadditive dispersion energy correlates well with the density of the system (Fig. 5) and is approximately proportional to $\rho^{2.5}$. Therefore, a set of Gibbs ensemble calculations are performed with a $\rho^{2.5}$ term included to model nonadditive dispersion using the form presented in Eq. (10). Including this term reduces the calculated enthalpy of vapor-

TABLE X. Nonadditive energies in a Gibbs ensemble simulation of CO_2 using a cut off distance of 14 Å. The coordinates are from simulations with the CBS-a potential. Values in parentheses are the uncertainties at the 95% confidence level.

	228 K	258 K	288 K
$E_{3,disp}$ (kJ mol^{-1})	1.01(0.005)	0.82(0.001)	0.63(0.001)
$E_{3,ind,iso}$ (kJ mol^{-1})	0.04(0.002)	0.03(0.001)	0.03(0.001)
$E_{3,ind,aniso}$ (kJ mol^{-1})	0.01(0.001)	0.01(0.001)	0.01(0.001)
$E_{3,exch}$ (kJ mol^{-1})	0.17(0.02)	0.08(0.006)	0.03(0.004)
$E_{3,tot}$ (kJ mol^{-1})	1.19(0.02)	0.92(0.006)	0.67(0.005)

Downloaded 02 Jul 2009 to 128.243.220.22. Redistribution subject to AIP license or copyright; see http://jcp.aip.org/jcp/copyright.jsp

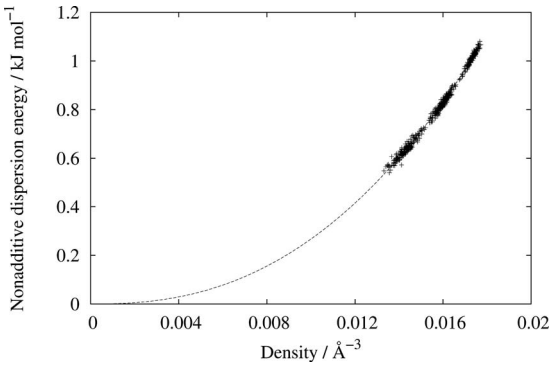

FIG. 5. Density dependence of the nonadditive dispersion energy. The equation of the dotted line is $(E/\text{kJ mol}^{-1})=2.55\times10^4\times(\rho/\text{Å}^{-3})^{2.5}$.

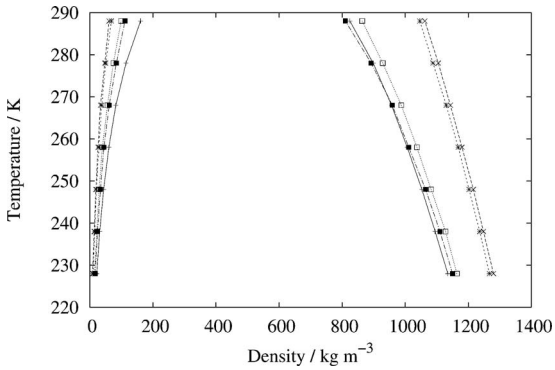

FIG. 6. Liquid-vapor coexistence densities from experiment (+) and calculated using the CBS-i (×), CBS-a (∗), nonadditive CBS-i (□), and nonadditive CBS-a (■) potentials.

ization by about 3 kJ mol^{-1} at all temperatures (Table XI). Nonadditivity also leads to a substantial improvement in the calculated phase coexistence densities (Fig. 6) and pressures.

Nonadditive dispersion only contributes ~1 kJ mol^{-1} to the internal energy of the system, but the enthalpy of vaporization changes by ~3 kJ mol^{-1}. Nonadditivity also increases the pressure of the liquid phase by a value proportional to $\rho^{3.5}$. The density of the liquid phase must decrease to equalize the pressure of the two phases, which accounts for the improvements in the calculated pressures and densities. The lower density also leads to a reduction in the strength of the pairwise interactions in the liquid phase, which further reduces the enthalpy of vaporization. The best agreement with the experimental phase coexistence properties is obtained with the CBS-a potential with a nonadditive correction and this potential is recommended for further simulations of CO_2.

IV. CONCLUSIONS

We have shown that potentials fitted to MP2 calculations reproduce well the phase properties of CO_2 when anisotropy and nonadditivity are considered. Isotropic pairwise potentials overestimate the strength of the CO_2 interaction. The inclusion of anisotropic terms in the fitted potentials improves the fit to the dimer potential energy surface. Anisotropy also improves the reproduction of experimental phase properties, but the CO_2 is still too strongly bound.

A sum of functions to reproduce the nonadditive dispersion, induction, and exchange repulsion given in Eqs. (5), (6), and (8) reproduce the nonadditive energies from *ab initio* calculations on the CO_2 trimer well. The nonadditive components of CO_2 trimer energies are small when compared to the additive energies. However, in the case of nonadditive dispersion, these small effects combine to add a repulsive interaction that accounts for most of the difference between the phase properties calculated with pairwise additive potentials and the experimental values.

The procedures described here can be used to study the potential energy surfaces and phase properties of other compounds. Hydrofluorocarbons will be the next target, with the aim of studying their interaction with CO_2.

TABLE XI. The phase properties of CO_2 calculated with two effective nonadditive potentials. Values in parentheses are the uncertainties at the 95% confidence level.

	Experiment	CBS-i	CBS-a
$\Delta H_{\text{vap}}^{228}$ (kJ mol^{-1})	14.49	15.66(0.3)	15.23(0.03)
$\Delta H_{\text{vap}}^{258}$ (kJ mol^{-1})	12.07	13.35(0.04)	12.77(0.04)
$\Delta H_{\text{vap}}^{288}$ (kJ mol^{-1})	7.81	10.00(0.06)	9.12(0.06)
ρ_l^{228} (kg m^{-3})	1134.9	1164(3)	1150(2)
ρ_l^{258} (kg m^{-3})	1006.1	1037(3)	1011(4)
ρ_l^{288} (kg m^{-3})	824.4	863.7(6.8)	810.1(18.6)
ρ_g^{228} (kg m^{-3})	21.8	14.6(0.5)	16.8(0.4)
ρ_g^{258} (kg m^{-3})	60.2	39.9(1.1)	44.6(1.1)
ρ_g^{288} (kg m^{-3})	160.7	99.9(3.1)	111.3(3.2)
P_{228} (bar)	8.2	5.8(0.2)	6.5(0.1)
P_{258} (bar)	22.6	16.2(0.3)	17.5(0.4)
P_{288} (bar)	50.2	37.1(0.5)	37.9(0.7)

ACKNOWLEDGMENTS

We thank Tim Lillestolen for calculating the atomic polarizabilities, Igor Stepanov for performing some preliminary Gibbs ensemble simulations, Jonathan Hirst for critical reading of this manuscript, and Ke Jie for helpful discussions. We thank the University of Nottingham High-Performance Computing facility for providing the computer resources used in this study and the Engineering and Physical Sciences Research Council for funding (Grant No. EP/E06082X/1).

[1] M. Poliakoff and P. King, Nature (London) **412**, 125 (2001).
[2] Y. Suehiro, M. Nakajima, K. Yamada, and M. Uematsu, J. Chem. Thermodyn. **28**, 1153 (1996).
[3] J. P. Hansen and I. R. McDonald, *Theory of Simple Liquids*, 2nd ed. (Academic, Boston, 1986).
[4] L. A. Webster and A. J. Kidney, J. Chem. Eng. Data **46**, 759 (2001).
[5] J. G. Harris and K. H. Yung, J. Phys. Chem. **99**, 12021 (1995).
[6] J. Vorholz, V. Harismiadis, B. Rumpf, A. Panagiotopoulos, and G. Maurer, Fluid Phase Equilib. **170**, 203 (2000).
[7] S. Bock, E. Bich, and E. Vogel, Chem. Phys. **257**, 147 (2000).
[8] R. Bukowski, J. Sadlej, B. Jeziorski, P. Jankowski, and K. Szalewicz, J. Chem. Phys. **110**, 3785 (1999).
[9] C. Bratschi, H. Huber, and D. J. Searles, J. Chem. Phys. **126**, 164105 (2007).
[10] M. J. Elrod and R. J. Saykally, Chem. Rev. (Washington, D.C.) **94**, 1975 (1994).
[11] G. Marcelli and R. J. Sadus, J. Chem. Phys. **111**, 1533 (1999).
[12] R. Bukowski and K. Szalewicz, J. Chem. Phys. **114**, 9518 (2001).

Downloaded 02 Jul 2009 to 128.243.220.22. Redistribution subject to AIP license or copyright; see http://jcp.aip.org/jcp/copyright.jsp

[13] A. E. Nasrabad, R. Laghaei, and U. K. Deiters, J. Chem. Phys. **121**, 6423 (2004).
[14] E. M. Mas, R. Bukowski, and K. Szalewicz, J. Chem. Phys. **118**, 4404 (2003).
[15] J. Li, Z. Zhou, and R. J. Sadus, J. Chem. Phys. **127**, 154509 (2007).
[16] H.-J. Werner, P. J. Knowles, R. Lindh *et al.*, MOLPRO, Version 2006.1, a package of *ab initio* programs, 2006.
[17] R. Kendall, T. Dunning, and R. Harrison, J. Chem. Phys. **96**, 6796 (1992).
[18] D. Woon and T. Dunning, J. Chem. Phys. **103**, 4572 (1995).
[19] G. Herzberg, *Molecular Spectra and Molecular Structure. II. Infrared and Raman Spectra of Polyatomic Molecules* (Van Nostrand Reinhold, Princeton, NJ, 1945).
[20] S. L. Price, A. J. Stone, and M. Alderton, Mol. Phys. **52**, 987 (1984).
[21] V. F. Lotrich and K. Szalewicz, J. Chem. Phys. **106**, 9668 (1997).
[22] B. M. Axilrod and E. Teller, J. Chem. Phys. **11**, 299 (1943).
[23] T. Lillestolen and R. Wheatley, J. Phys. Chem. A **111**, 11141 (2007).
[24] R. J. Wheatley, Mol. Phys. **84**, 899 (1995).
[25] A. Z. Panagiotopoulos, Mol. Phys. **61**, 813 (1987).
[26] M. H. Champagne, X. Li, and K. L. C. Hunt, J. Chem. Phys. **112**, 1893 (2000).

Downloaded 02 Jul 2009 to 128.243.220.22. Redistribution subject to AIP license or copyright; see http://jcp.aip.org/jcp/copyright.jsp